International Journal of Heat and Mass Transfer 60 (2013) 689–699

Contents lists available at SciVerse ScienceDirect

International Journal of Heat and Mass Transfer

journal homepage: www.elsevier.com/locate/ijhmt

Analytical and numerical parameter extraction for compact modeling of thermoelectric coolers

Min Chen [a,*], G. Jeffrey Snyder [b]

[a] Department of Energy Technology, Aalborg University, Pontoppidanstræde 101, DK-9220 Aalborg, Denmark
[b] Materials Science, California Institute of Technology, Pasadena, CA 91125, USA

ARTICLE INFO

Article history:
Received 22 July 2012
Received in revised form 3 December 2012
Accepted 9 January 2013
Available online 14 February 2013

Keywords:
Thermoelectric cooler
Peltier effect
Compact modeling
Thermal management
CFD

ABSTRACT

The 3D compact model of a thermoelectric cooler in the CFD approach is an essential technique for computationally realistic design of many industrial thermal management applications. The first objective of this paper is to develop a "black box"-like model for thermoelectric coolers as well as a method to formulate the effective material properties for the compact model based on the manufactures' datasheets. Second, a highly detailed and physical thermoelectric cooler model is implemented to carry out virtual experiments when the cooler datasheet is not available. A number of close comparisons validate that the compact model and parameter extraction are accurate enough, and the computation time and size are significantly lower than the physical model. The compact model is also demonstrated to be helpful in evaluating the thermal system components such as an air-cooled heat sink, so that the system-level thermal management optimization is possible without complex, multi-scale computation.

1. Introduction

Thermoelectric cooling technology can reduce the temperatures of electronic module packages below the ambient environment temperature without the use of pumped liquid cooling or vapor-compression refrigeration. The solid state refrigerators are hence particularly appropriate to the growing situation of cooling where reliability, volume and complexity are of prior consideration to the cooling coefficient of performance (COP). In addition, the stringent temperature control required by some optoelectronic components can also be provided by thermoelectric coolers (TECs), the cooling of which is readily controlled through adjusting the current applied. A constant temperature or heat flux of the TEC can be maintained by the tight thermal management even if the ambient thermal condition around it varies dynamically. For these benefits, there has been an increased interest in the application of TECs to electronic and photonic device cooling to handle the heat from the high power density devices, and TECs have actually been used in many diverse applications for extending the ability of air/liquid-cooled heat sinks [1–8].

The successful design of a thermoelectric cooling system necessitates an excellent TEC simulation, which ideally should be able to analyze the cooling performance and predict the thermal behavior with sufficient accuracy. A number of three-dimensional (3D) TEC models have been reported, in which the geometric detailed representation of the entire array of thermoelements is exactly modeled [9–13]. However, these TEC models are not developed within computational fluid dynamics (CFD) software packages, and hence difficult to be integrated into a larger system-level analysis against the fluidic heat exchange. Also based on the true solid representation of the thermoelectric device, other 3D models have been implemented by the original approach for a CFD simulation, making the co-simulation of thermoelectric devices and fluid heat sources convenient [14,15]. In [15], the popular CFD code FLUENT is numerically equipped with a thermoelectric model for generation applications, where the temperature dependence of all properties of the *p*- and *n*-type materials, the thermo-electric coupled multiphysics field, and the complete thermoelectric processes of Seebeck, Peltier, and Thomson effects integrated with Joule source terms, are all taken into account.

The integration of thermoelectric devices into CFD simulation environments is also of interest. Here a major interest and concern from industry is the practicality and cost of modeling. While the multiphysics packages are ideal for modeling each *n*-type and *p*-type element, thermal and electrical contact individually [9–15], the cell/grid size should be on the order of microns to accurate calculate the thermoelectric device. The ideal cell/grid size for the system is typically orders of magnitude larger introducing "grid mismatch" making integration of the multiphysics model of a TE with a system model very computationally expensive and complicated to perform.

Modeling the TE module as a single bulk block or "black box" to represent the TEC instead of modeling each thermoelement

* Corresponding author. Tel.: +86 13439685281.
E-mail address: chenminmike@gmail.com (M. Chen).

0017-9310/$ - see front matter © 2013 Elsevier Ltd. All rights reserved.
http://dx.doi.org/10.1016/j.ijheatmasstransfer.2013.01.020

Nomenclature

A	uniform cross-sectional area of the entire TEC, m^2
A_p	uniform cross-sectional area of p-type leg, m^2
A_n	uniform cross-sectional area of n-type leg, m^2
CFD	computational fluid dynamics
COP	coefficient of performance
f	packing fraction of total TEC area covered by thermoelectric elements
i	reduced current
I	electrical current, A
I_{max}	the electrical current in the device that gives ΔT_{max}, A
K	effective thermal conductance of the TEC, $W K^{-1}$
K_l	effective parallel thermal conductance within the TEC of one pair of thermoelements, $W K^{-1}$
l	thermoelectric element length or height, m
L	height of the macro block (l plus the height of the top and bottom metal interconnects), m
N	number of couples in the TEC module
q_{joule}	the Joule heating density, W/m^3
q_{pelt}	the Peltier heat generation rate, W/m^3
$\dot{Q}$	the rate of heat transfer at the side being cooled, W
$\dot{Q}_{max}$	the maximum rate of heat transfer at the side being cooled with no temperature difference, W
Q_c	total rate of heat transfer from the heat source, W
Q_h	total rate of heat transfer to the heat sink, W
R	electrical resistance of the TEC, Ω
R_l	effective parasite resistance of one pair of thermoelements, Ω
S	$=2n\alpha$, effective lumped Seebeck coefficient of the TEC black box, $V K^{-1}$
T	temperature, K
T_c	temperature of the TEC cold side, K
T_h	temperature of the TEC hot side, K
T_{ci}	cold junction temperature, K
T_{hi}	hot junction temperature, K
TEC	thermoelectric cooler
V	voltage of external power supply, V
z_p	p-type material figure of merit
i	n-type material figure of merit
Z	effective device figure of merit

Greek symbols

α	effective Seebeck coefficient of the compact TEC model, $V K^{-1}$
α_p	Seebeck coefficient of the p-type materials, $V K^{-1}$
α_n	Seebeck coefficient of the n-type materials, $V K^{-1}$
ΔT	$=T_h - T_c$, external temperature difference between the hot and cold sides, K
ΔT_{max}	the maximum temperature difference when there is no heat absorbed at the cold side, K
ΔT_{TE}	$=T_{hi} - T_{ci}$, internal temperature difference between the hot and cold junctions, K
κ	effective thermal conductivity of the compact TEC model, $W m^{-1} K^{-1}$
κ_l	effective parallel thermal conductivity within the TEC of one pair of thermoelements, $W m^{-1} K^{-1}$
κ_p	thermal conductivity of the p-type semiconductor material, $W m^{-1} K^{-1}$
κ_n	thermal conductivity of the n-type semiconductor material, $W m^{-1} K^{-1}$
ρ	effective electrical resistivity of the compact TEC model, Ω m
ρ_l	effective parasite electrical resistivity of one pair of thermoelements, Ω m
ρ_p	electrical resistivity of the p-type semiconductor material, Ω m
ρ_n	electrical resistivity of the n-type semiconductor material, Ω m
γ_p	$=\frac{A_p}{A_n+A_p}$, relative area for the p-type thermoelectric elements
γ_n	$=\frac{A_n}{A_n+A_p}$, relative area for the n-type thermoelectric elements
Θ_c	cold substrate, $W^{-1} K$
Θ_h	hot substrate, $W^{-1} K$

individually can make the computation much easier [16–23]. This kind of compact models is able to cope with the multiscale issue at the interface between the very fine mesh of the thermoelement region and relatively coarse mesh of the package and fluid region. Because the TEC module as a whole rather than each pellet is modeled, the TEC gridding can be significantly simplified and the grid mismatch can thus be mitigated. From a computational efficiency standpoint, full-field CFD and heat transfer simulations are now less expensive but more feasible as the number of volumes as well as the algorithm complexity is reduced. In applying compact TEC models, however, retaining the accuracy in capturing the cooling performance is as important as the simulation simplicity.

It is noteworthy that the model parameters have decisive influence on the simulation results. Thus, the process of parameter procurement is inextricable to the method of building a compact model itself, and actually a key design step in the model construction. The critical technique here is how to determine the effective values of κ, ρ, and α for the compact TEC model in a prompt and easy manner. In this concern, the convenient parameter extraction methodology utilizing manufacture's published data [24] has been widely extended in one dimensional (1D) TEC modeling and design [25–27]. The method does not require additional information except the readily available datasheet to produce the TEC performance against applied conditions. However, this method only extracts 1D lumped parameters of the TEC module such as thermal and electrical resistance, but does not give the effective material properties for the 3D compact model. So far, a comprehensive co-design methodology of compact modeling and parameter extraction of TECs in the CFD approach has not been available.

This paper presents a compact TEC model running on the commercially available CFD code FLUENT, on which the innumerous thermal management models already existing can be efficiently integrated with TECs. The compact model is accompanied with an analytical scheme of parameter extraction, where only four parameters from TEC manufacturers' datasheets (ΔT_{max}, I_{max}, $\dot{Q}_{max}$, T_h) are used to characterize κ, ρ, and α of the "black box", whilst other information of the device is not required. In order to generalize the methodology, the detailed model of thermoelectric generators [15] is extended to be a TEC model with full thermocouple geometry. The physical TEC model is then used to virtually extract the effective κ, ρ, and α of the compact model for the general scenario where all TEC parameters are completely available. The physical model and the compact model give almost exactly the same result, but in combination with an air-cooled heat exchanger as an example analyzing cooling enhancement, the latter improves the computation efficiency significantly.

2. Compact TEC model and analytical parameter extraction

A typical TEC module is shown in Fig. 1(a), in which many n- and p-type semiconductor legs composing the cooler are connected

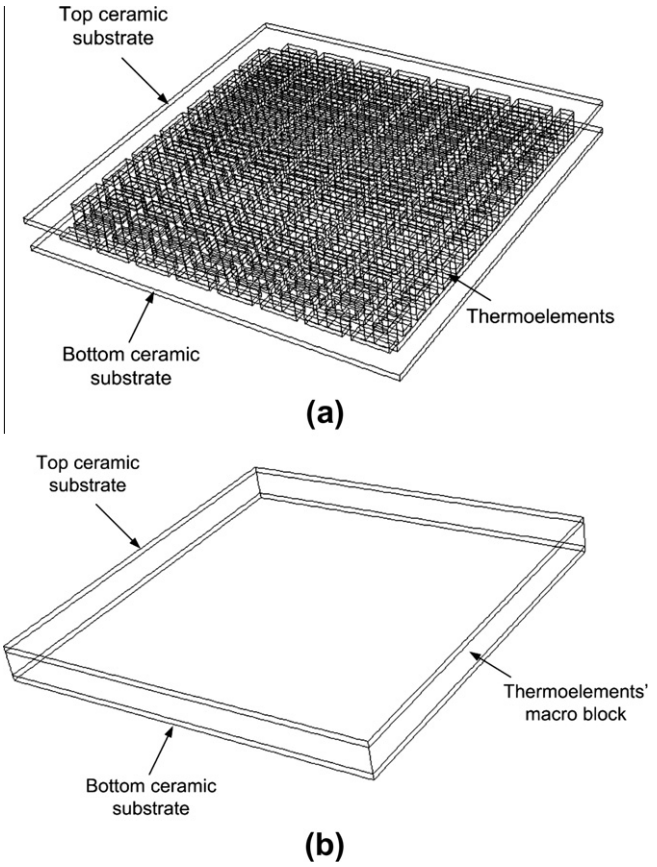

Fig. 1. TEC module. (a) Detailed full geometry. (b) Compact modeling scheme.

thermally in parallel between the hot and cold ceramic substrates, and electrically in series by the interconnect metals to receive the current from the external power supply. Due to the thermoelectric effects, heat is removed from the cold side of the TEC, which is attached to the object to be cooled, while the TEC hot side dissipates heat to the ambient. The net effect is that a temperature gradient is created within the TEC.

Fig. 1(b) presents the compact scheme of the full model in Fig. 1(a). There are only three sections, in which the bottom and top blocks correspond to two ceramic substrates, and the macro block in the middle represents all thermoelements and the interconnect metal bridges above and below the *n*- and *p*-type elements of thermoelectric material. Compared with using the detailed geometry, the compact model is obviously advantageous for carrying out computationally intensive parametric studies across various length scales during system prototype design. However, as the compact model greatly simplifies the complicated TEC device structure into a regular cuboid careful extraction and implementation of the effective κ, ρ, and α are critical to ensure the block to faithfully characterize the TEC.

The characteristics of a particular TEC that define its performance are $\Delta T_{\max}$, $I_{\max}$, and $\dot{Q}_{\max}$ (defined explicitly below). While the thermoelectric materials ZT primarily determines $\Delta T_{\max}$, the extensive values $I_{\max}$, and particularly $\dot{Q}_{\max}$ depend on the device size, primarily through the area A, and height l, of the TEC. For optimum sizing of a TEC, it is convenient to formulate the heat flow equations so that the adjustable geometric variables are separated from the internal, fixed material and device properties. In the following analysis, the effects of the hot and cold substrates are not immediately included to directly utilize $\Delta T_{\max}$, $I_{\max}$, and $\dot{Q}_{\max}$ etc, specified by the TEC manufacturer. The effect of substrates will be discussed at the end of the analysis, as an additional thermal conduction element.

We start with the traditional formulation for TEC by assuming temperature independent properties of thermoelectric materials. The rate of heat being removed from the object being cooled (with temperature T_c) of the TEC is written as,

$$\dot{Q} = SIT_c - K\Delta T - \frac{1}{2}I^2R, \tag{1}$$

where the three terms at the right side represent the contribution of the Peltier effect, the heat conduction, and the Joule effect, respectively [28]. Although the temperature dependence of material properties can be significant in the evaluation of thermoelectric device performance [15], the common assumption of constant material attributes made in compact TEC models usually does not give rise to a main source of error because the temperature gradient in TEC is not so large when compared with the case of thermoelectric generators unless operating near $\Delta T_{\max}$. When the thermal load $\dot{Q}$ is large, the side being cooled may actually be at a higher temperature than the side being heated, making $\Delta T < 0$. This is also the case when the TEC is working as a power generator.

The electrical current in the device that gives the maximum ΔT can be obtained by the derivative of ΔT with respect to I using (1),

$$\frac{d\Delta T}{dI} = 0 \Rightarrow I_{\max} = \frac{ST_c}{R}. \tag{2}$$

When $\dot{Q} = 0$,

$$\Delta T_{\max} = \frac{S^2T_c^2}{2KR}. \tag{3}$$

Substituting $I_{\max}$ into (1) yields

$$\dot{Q} = \frac{S^2T_c^2}{2R} - K\Delta T. \tag{4}$$

$\dot{Q}_{\max}$ of the TEC is the $\dot{Q}$ achieved when $\Delta T = 0$. It is found to be

$$\dot{Q}_{\max} = \frac{S^2T_c^2}{2R}. \tag{5}$$

At this point the parameters needed for calculation of the performance of the cooler (S, K, and R in Eq. (1)) can be determined from the appropriately defined specifications of cooler performance ($\Delta T_{\max}$, $I_{\max}$, $\dot{Q}_{\max}$ and the ambient temperature T_h). $K = \frac{\dot{Q}_{\max}}{\Delta T_{\max}}$ and $R = 2\frac{\dot{Q}_{\max}}{I_{\max}^2}$ and $S = 2\frac{\dot{Q}_{\max}}{I_{\max}}\frac{1}{T_h - \Delta T_{\max}}$.

$\Delta T_{\max}$ can be further solved giving $\Delta T_{\max}$ in terms of T_h which is more commonly controlled than T_c in a TEC,

$$\Delta T_{\max} = \frac{ZT_h^2}{1 + ZT_h + \sqrt{1 + 2ZT_h}}. \tag{6}$$

Equation (1) is succinctly rewritten in terms of the extensive variables relative to their maximum quantities to obtain (again for constant T_c as opposed to the more commonly used constant T_h)

$$\frac{\dot{Q}}{\dot{Q}_{\max}} = \frac{I}{I_{\max}}\left(2 - \frac{I}{I_{\max}}\right) - \frac{\Delta T}{\Delta T_{\max}}. \tag{7}$$

2.1. Internal model of TEC

When the intensive TEC material properties are known or desired, they can be related to the extensive properties of the TEC (S, K, and R). $S = 2N\alpha$ where $2\alpha = \alpha_p - \alpha_n$. Note that for similar n and p-type thermoelectric materials $\alpha_n \approx -\alpha_p$, and α can then approximately be the average thermopower of the thermoelectric materials ($\alpha = \frac{1}{2}\alpha_p - \frac{1}{2}\alpha_n \approx \alpha_p$).

The TEC thermal conductance, K, can be considered the sum of all the parallel thermal conductance paths between the hot and cold sides,

$$K = N\left(\frac{\kappa_n A_n}{l} + \frac{\kappa_p A_p}{l} + K_l\right). \tag{8}$$

Here K_l is the compilation of parallel thermal losses associated with the underfill, egg-crate, radiation, gas conduction etc., per couple. The relative area $\gamma_{p,n}$ is fixed by optimizing TEC performance. The total TEC area, A, depends not only on the number of couples, N and the area of the thermoelectric elements $A_n + A_p$, but also f, the fraction of A covered by the TE elements of the TEC,

$$Af = N(A_n + A_p). \tag{9}$$

Thus K can be simplified to

$$K = \frac{Af}{l}\kappa, \tag{10}$$

where

$$\kappa = \kappa_n \gamma_n + \kappa_p \gamma_p + \kappa_l, \tag{11}$$

with $\kappa_l = \frac{nl}{Af} K_l$ again due to parallel thermal conduction losses. $\gamma_p = \frac{A_p}{A_n + A_p}$ and $\gamma_n = \frac{A_n}{A_n + A_p}$ are the relative areas for the p-type and the n-type thermoelectric elements, respectively. Note that for similar n and p-type thermoelectric materials, κ is approximately the thermal conductivity of the thermoelectric materials $\left(\kappa = \frac{1}{2}\kappa_n - \frac{1}{2}\kappa_p \approx \kappa_p\right)$.

Similarly, R is the sum of the resistances of the n- and p-type elements, and contact plus strap (interconnect), R_l, per couple,

$$R = N\left(\frac{\rho_n l}{A_n} + \frac{\rho_p l}{A_p} + R_l\right). \tag{12}$$

The resistance simplifies to

$$R = \frac{N^2 l}{Af} 4\rho, \tag{13}$$

where

$$4\rho = \frac{\rho_n}{\gamma_n} + \frac{\rho_p}{\gamma_p} + R_l, \tag{14}$$

with $\rho_l = \frac{Af}{Nl} R_l$. Note that for similar n and p-type thermoelectric materials, ρ is approximately the effective resistivity of the thermoelectric materials $\left(\rho \approx \frac{1}{4}\left(\frac{\rho_n}{1/2} + \frac{\rho_p}{1/2}\right) \approx \rho_p\right)$.

The $I_{\max}$ of Eq. (2) is

$$I_{\max} = \frac{Af}{Nl}\frac{\alpha T_c}{2\rho}, \tag{15}$$

and $\Delta T_{\max}$ of Eq. (3) is

$$\Delta T_{\max} = \frac{ZT_c^2}{2}, \tag{16}$$

where $Z = \frac{\alpha^2}{\rho\kappa}$ approaches $z_{p,n} = \frac{\alpha_{p,n}^2}{\rho_{p,n}\kappa_{p,n}}$ when there are no electrical or thermal losses, and similar n and p-type thermoelectric materials assuming temperature independent properties.

Using the average material parameters, Eq. (1) is succinctly rewritten in terms of the reduced current i,

$$i = \frac{I}{I_{\max}} \tag{17}$$

to obtain (for constant T_c)

$$\dot{Q} = \frac{Af}{l}\left(\frac{\alpha^2 T_c^2}{\rho}\left(i - \frac{i^2}{2}\right) - \kappa\Delta T\right). \tag{18}$$

When $i = 1$, $\Delta T = 0$, $\dot{Q}_{\max}$ is obtained,

$$\dot{Q}_{\max} = \frac{Af}{l}\frac{\alpha^2 T_c^2}{2\rho}. \tag{19}$$

Note that unlike $\dot{Q}_{\max}$, $\Delta T_{\max}$ does not scale with any device geometric parameter (A, l, f, or N), it is only a function of the materials properties through the thermoelectric figure of merit. The heat flux ($\dot{Q}/A$) however scales with the packing fraction and length (f/l) and not with the number of elements n. The number of elements only becomes important when the absolute current (as opposed to reduced current i) or resistance is needed. The current scales as Af/Nl, (Eq. (15)) while the resistance scales as $N^2 l/Af$. The N^2 scaling of resistance is necessary because a doubling of the number of thermoelectric elements (keeping area and filling fraction constant) requires also a halving of the area of each element, which doubles the resistance per element.

The effective average thermoelectric properties α, ρ, κ, can now be derived from manufacturer $\Delta T_{\max}$, $I_{\max}$, $\dot{Q}_{\max}$ specifications and TEC geometry (A and l) using a reformulation of the mathematic expressions (15), (16), and (19) as long as the filling fraction f (typically about 0.25) and number of couples N are assumed, namely:

$$\alpha = \frac{\dot{Q}_{\max}}{NT_c I_{\max}}, \tag{20}$$

$$\rho = \frac{Af}{2l}\frac{\dot{Q}_{\max}}{N^2 I_{\max}^2}, \tag{21}$$

$$\kappa = \frac{l}{Af}\frac{\dot{Q}_{\max}}{\Delta T_{\max}}. \tag{22}$$

However, the mathematic manipulation above must be calibrated because of the different measurements of T_c in $\Delta T_{\max}$, $I_{\max}$, and $\dot{Q}_{\max}$. As is stated, the condition in determining $\dot{Q}_{\max}$ in (5) and (19) is $\Delta T = 0$, i.e., $T_h = T_c$, whilst the objective of $I_{\max}$ is to maximize ΔT, i.e., to achieve $\Delta T_{\max}$. Since TEC performance data are commonly published for constant hot side temperatures (usually 27 °C and 50 °C), (19), e.g., is changed to

$$\dot{Q}_{\max} = \frac{Af}{l}\frac{\alpha^2 T_h^2}{2\rho}, \tag{23}$$

in order to conform with the expressions of $I_{\max}$ and $\dot{Q}_{\max}$, where $T_c = T_h - \Delta T_{\max}$. Combining (15), (16), and (23) yields

$$\alpha = \frac{\dot{Q}_{\max}(T_h - \Delta T_{\max})}{NT_h^2 I_{\max}}, \tag{24}$$

$$\rho = \frac{Af(T_h - \Delta T_{\max})^2}{2T_h^2 l}\frac{\dot{Q}_{\max}}{N^2 I_{\max}^2}, \tag{25}$$

$$\kappa = \frac{l(T_h - \Delta T_{\max})^2}{AfT_h^2}\frac{\dot{Q}_{\max}}{\Delta T_{\max}}. \tag{26}$$

In (24)-(26), $\Delta T_{\max}$, $I_{\max}$, $\dot{Q}_{\max}$, and T_h are directly available from the TEC vendor. The number of elements and element dimensions can also be easily derived from the device diagram in datasheets or measured from the real module. Thus, the effective material properties α, ρ, κ, for the compact model are successfully extracted.

In the above formulation, parallel heat loses due to K_l can simply be included by increasing κ. In a real TEC there is also thermal resistance between the external surfaces of the TEC and the internal junction between the thermoelectric materials and the interconnect metals. As is shown in Fig. 2, all the series thermal resistances between the external cold temperature measurement (T_c) and the internal thermoelectric material cold junction temperature (T_{ci}) are summed together to give Θ_c. This may include thermal resistances from the substrate, interconnects, thermal contact

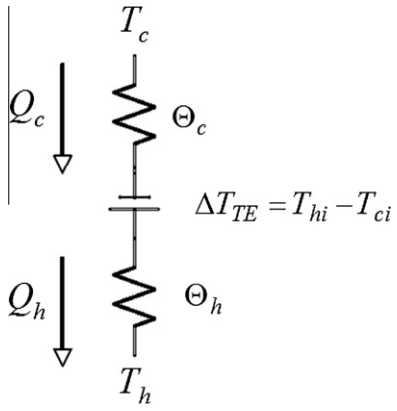

Fig. 2. 1D heat transfer analogy from the heat source to the heat sink.

resistance and substrate spreading resistance. Similarly defined on the hot side are T_h, T_{hi}, and Θ_h.

The importance of these thermal resistances depends on their relative magnitude compared to the thermal resistance of the thermoelectric material. Thus these additional thermal resistances become more important as the height of the thermoelectric elements is decreased. However, Θ_c and Θ_h are usually unknown in manufacturers' datasheets, so the maximum of the internal temperature difference, ΔT_{TE}, cannot be obtained from the published external $\Delta T_{\max}$. Moreover, the current value $I_{\max}$ which maximizes $T_h - T_c$, does not necessarily maximize $T_{hi} - T_{ci}$.

We notice that $\Delta T_{\max}$, $I_{\max}$, $\dot{Q}_{\max}$ and T_h in datasheets are external performance parameters measured for the entire TEC, where the effects of Θ_c and Θ_h are included. When one is evaluating TEC through a compact model, the main concern is to evaluate parameters that reproduce device performance accurately. Therefore, in this compact model, the effective α, ρ, κ of the main block containing the thermoelectric materials as opposed to the top/bottom layers are directly calculated by manufacturers' $\Delta T_{\max}$, $I_{\max}$, $\dot{Q}_{\max}$ and T_h using (24)-(26). In this way, all thermal and electrical properties of the TEC, reflected by the performance parameters, are assumed to result entirely from the thermoelectric layer. To test these values in the model, a very large thermal conductivity, much larger than the ceramic material, is applied to the top and bottom substrates of the test structure to essentially eliminate the effect of the thermal resistances Θ_c and Θ_h. Because very large values of conductivity inhibit rapid convergence of the calculation, a value of 200 W m^{-1} K^{-1} is applied to the two substrates in the test cases.

The 3D TEC model is implemented in the 64 bit ANSYS FLUENT 12.1. User-defined functions (UDFs) are used to model the effective heat conduction, volumetric Joule heat source, and interfacial Peltier heat in terms of α, ρ, κ extracted from $\Delta T_{\max}$, $I_{\max}$, $\dot{Q}_{\max}$ and T_h in datasheets. The UDF for the effective conductivity of the TEC materials is implemented in terms of (26) to model the Fourier heat flow in the middle TE block.

An energy_source UDF is written to uniformly generate the volumetric Joule heat on all cells of the middle block. By combing (13) and (25), the Joule heating density can be obtained as

$$q_{joul} = \frac{I^2 R}{AL} = \frac{I^2}{AL}\frac{N^2 4\rho l}{Af} = i^2 \frac{2(T_h - \Delta T_{\max})^2 \dot{Q}_{\max}}{ALT_h^2}, \tag{27}$$

where $I(i)$ can be determined as the model input parameter representing the electrical current applied to the TEC.

The Peltier heat is absorbed and evolved at the cold and hot junctions of dissimilar materials, respectively. In the compact model, two Peltier UDFs are used to represent the absorbed and evolved heat, and placed at the two interfaces between the middle

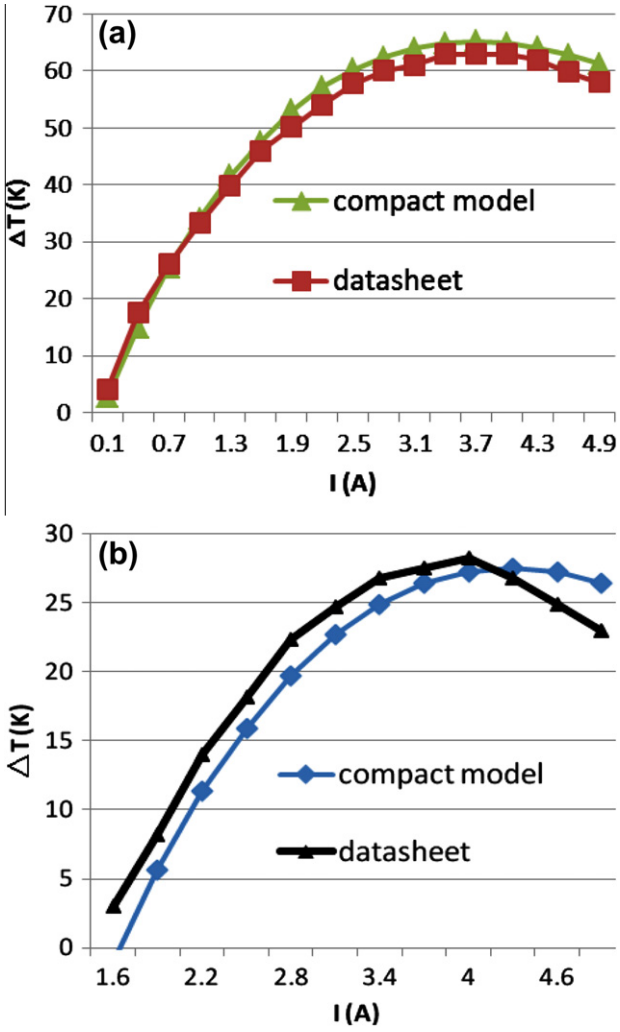

Fig. 3. TEC temperature difference comparison between compact simulation and datasheet for various currents (a) $\dot{Q} = 0$ W, $T_h = 300$ K; (b) $\dot{Q} = 20$ W, $T_h = 300$ K.

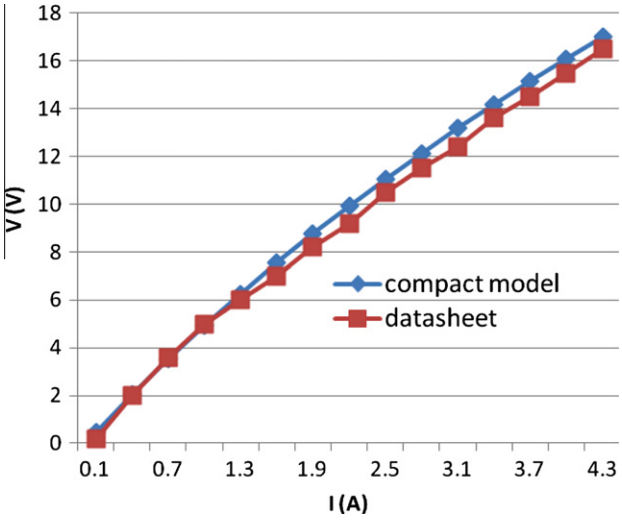

Fig. 4. TEC power supply voltage comparison between compact simulation and datasheet for various currents ($\dot{Q} = 0$ W, $T_h = 300$ K).

TE block and the bottom/top substrates as their boundary profiles. FLUENT is able to solve a 1D conduction equation of the interfacial walls as well as the heat generation in the wall. To include Peltier

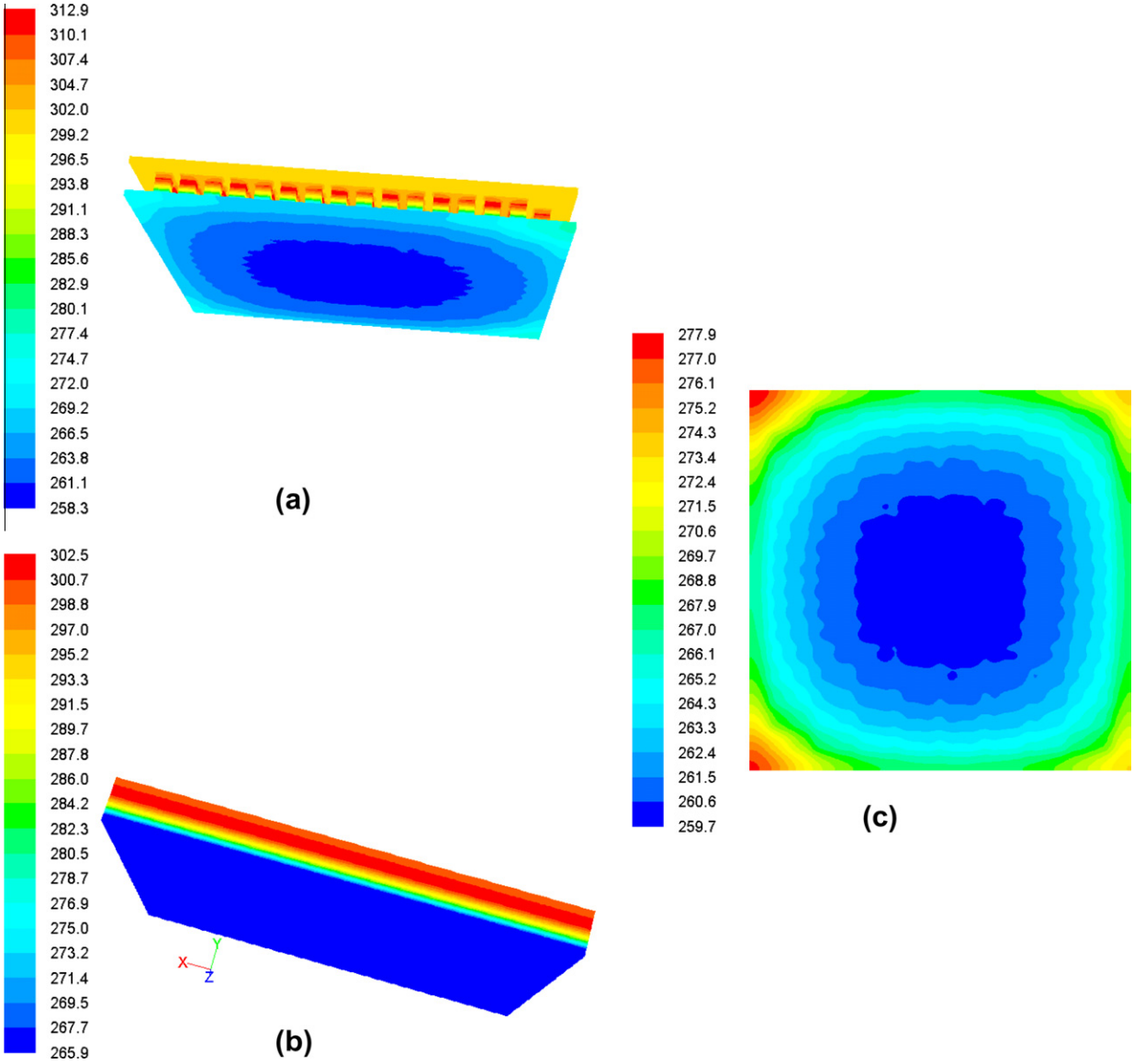

Fig. 5. Temperature contours of (a) 3D physical TEC model, (b) 3D compact TEC model, (c) 2D cold side by physical TEC model. (Unit: K, $\dot{Q} = 20$ W, $T_h = 300$ K, $I = 5.7$ A).

Table 1
Summary of the physical TEC model.

Zone type	Material	Source terms	Potential fields	Solid number
p-Type leg	*p*-Type thermoelectric material	Joule; Thomson; Peltier	Seebeck; Ohm	127
n-Type leg	*n*-Type thermoelectric material	Joule; Thomson; Peltier	Seebeck; Ohm	127
Top bridge	Conducting metal	Joule	Ohm	127
Bottom bridge	Conducting metal	Joule	Ohm	126
Bottom bridge (+)	Conducting metal	Joule	Ohm	1
Bottom bridge (−)	Conducting metal	Joule	Ohm	1
Substrate	Ceramic			2

effects in the heat transfer calculation, the thickness of the wall is specified as 10^{-5} m. We note that a non-zero thickness must be specified in FLUENT for such thin wall thermal calculation, even though this thickness does not really exist in the solid model. By using (24), the heat generation rate due to Peltier effect can be obtained as

$$q_{pelt} = \pm\frac{N2\alpha IT_{hi,ci}}{A^*10^{-5}} = \pm\frac{\dot{Q}_{\max}(T_h - \Delta T_{\max})}{NT_h^2 I_{\max}}\frac{N2IT_{hi,ci}}{A^*10^{-5}} = \pm i\frac{\dot{Q}_{\max}(T_h - \Delta T_{\max})2T_{hi,ci}}{T_h^2 A^*10^{-5}}, \quad (28)$$

where the plus and minus signs stipulate whether the Peltier heat is evolved or absorbed. The UDFs are able to identify the interfaces and external surfaces automatically, and hence calculate the average T_h, T_c, T_{hi} and T_{ci} at the four surfaces as the simulation results. Both the internal ΔT_{TE} and the external ΔT can be similarly calculated at the end of each iteration, and V is also obtained in terms of the internal ΔT_{TE},

$$V = S\Delta T_{TE} + RI. \quad (29)$$

In order to validate the compact model as well as the parameter extraction method, the TEC DT12-4 made by Marlow is simulated as the example. The TEC has 127 thermocouples ($N = 127$) and a $30 * 30$ mm^2 cross-section, and hence a filling factor of 0.2822.

The four key performance parameters are described in the manufacturer's datasheet when the hot temperature is fixed at 300 K, i.e., ΔT_{max} = 66 K, I_{max} = 3.7 A, $\dot{Q}_{max}$ = 36 W [29]. Substituting these values into (24)-(26), effective material properties for the compact model can be obtained, i.e., α = 199 μ V/K, ρ = 13 μ Ω m, κ = 1.31 W m^{-1} K^{-1}.

Fig. 3 and 4 compare performance curves published in the datasheet [29] and the simulation results of the compact model for T_h = 300 K. The scenario of zero thermal load (Q = 0 W) is presented in Fig. 3(a), where ΔT changes with I. Fig. 3(b) presents the case that $\dot{Q}$ = 20 W, which is closer to the realistic cooling applications. In Fig. 4, the change of V with I is depicted for comparison between the datasheet and the simulation. For most current values, it can be seen that the simulated ΔT and V match the datasheet's characteristics very well. The deviation becomes slightly obvious when $\dot{Q}$ is increased and when I passes its maximum value ($I > I_{max}$), likely caused by measurement uncertainties of performance parameters and the simplification of the compact modeling approach. However, given the benefits on computational cost brought by the compact model, such a small error level is fairly acceptable for practical cooling system design [16–23].

3. Physical TEC model and virtual parameter extraction

To determine quantitatively how much computational cost can be saved by using the compact model, it is necessary to compare the same TEC in a modeling approach that uses the full geometry. The 3D thermoelectric model in [15], validated by experimental results, is ideal for this purpose because it is also implemented in FLUENT, so that any comparisons should be computationally fair. Also, there may be a need to extract the effective material properties from the measured device properties used in the compact model, especially for those TECs under laboratory development and testing. Although manufacturer's specifications are a reliable data source, a full TEC model is important to evaluate also in the case when all material parameters, including the temperature dependency of α, ρ, κ, thermal and electrical contact resistance are given instead of the device performance. The full TEC model can be used to calculate ΔT_{max}, I_{max}, $\dot{Q}_{max}$ for a given T_h from the material properties and geometry.

As the 3D model in [15] faithfully includes all coupled thermoelectric as well as components that provide losses and other parasitic effects, it can be referred to as the physical model in contrast with the compact model which is only concerned with overall performance. The physical model used here was originally created for thermoelectric generators (TEG) [15], so the model should be transplanted for coolers as the first step. Due to the same governing equations of thermoelectricity for TEG and TEC, the numerical schemes and model framework are the same except that the concept of a load resistance of a TEG is replaced by the the current supplied I used for TECs.

The 3D physical model of a 127 couple (N = 127) TEC module is shown in Fig. 5(a) and the modeling domain is summarized in Table 1. The minus and plus pads, which used to simulate the lead wires of the TEG, are now used to pass through the prescribed I to establish the electric current density through the TEC. The current direction is applied in a way to ensure that Peltier heat is absorbed at the cooling side and released at the other.

In the physical TEC model, V of the external power supply is calculated as

$$V = \sum_N \left(\int_\Gamma \alpha_p \nabla T dr - \int_\Gamma \alpha_n \nabla T dr \right) + I \sum_N \left(\int_\Gamma \rho_p \nabla \frac{1}{A_p} dr + \int_\Gamma \rho_n \nabla \frac{1}{A_n} dr \right) + V_{strap}, \quad (30)$$

instead of (29), where the first term is the sum of Seebeck potential of all thermoelements working against I, and the second term is the ohmic voltage drop as I flows through all thermoelements of the TEC module. $\alpha_{p,n}$ and $\rho_{p,n}$ are dependent properties of the 3D temperature distribution T for each n- or p-type leg in the physical model. The starting and the end points of the curvilinear integral Γ depend on the actual contacts in the junctions between which the effective Seebeck potential and resistance of each leg are measured. In this model the voltage drop across the strap (V_{strap}) resistance of the bridges are also included by the continuous potential field although not described in detail in (30).

Similarly, the full 3D temperature field of the TEC can be established by the physical model, as is shown in Fig. 5(a), in which the I-related source terms of Peltier, Thomson, and Joule heat are all included. The TEC thermal load $\dot{Q}$ in the physical model consists of the absorbed Peltier heat subtracted by the nonlinearly conducted heat from the hot side, i.e.,

$$\dot{Q} = \sum_N \left(\iiint_\Omega \nabla \alpha_p T J d\Omega + \iiint_\Omega \nabla \alpha_n T J d\Omega - \iint_{A_p} -\kappa_p \nabla T dA_p - \iint_{A_n} -\kappa_n \nabla T dA_n \right), \quad (31)$$

where $\alpha_{p,n}$ and $\kappa_{p,n}$ are dependent properties of T for each n- or p-type leg. The volume integral Ω and the surface integral $A_{p,n}$ are with respect to Peltier heat density and the conduction heat flux at the n- or p-type cold junctions.

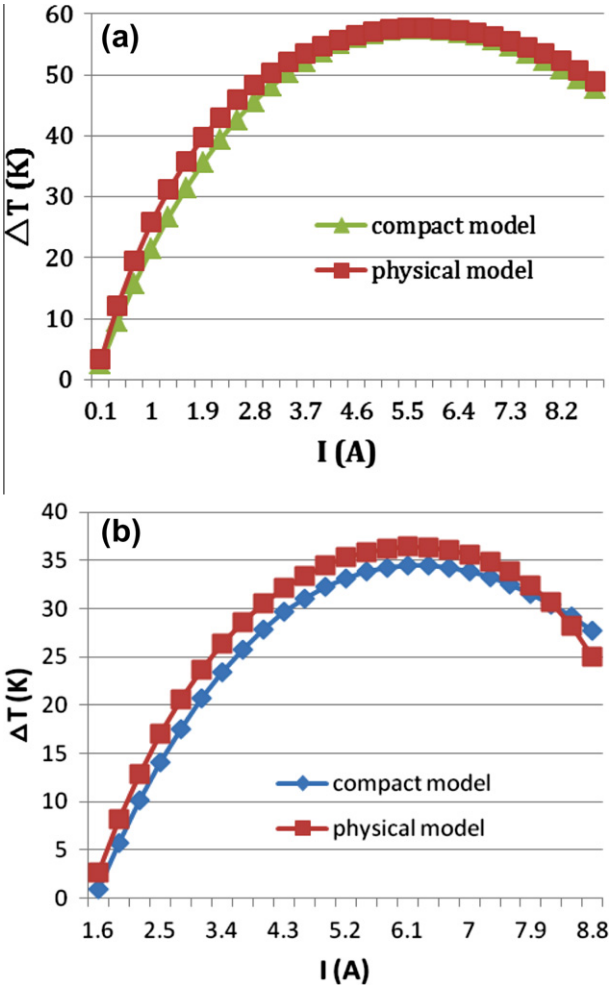

Fig. 6. TEC temperature difference comparison between compact simulation and full simulation for various currents (a) $\dot{Q}$ = 0 W, T_h = 300 K.(b) $\dot{Q}$ = 20 W, T_h = 300 K.

Within FLUENT, the 3D physical model solves the nonlinearly coupled thermal and electrical processes such as (30)-(31) for the components in Tabel 1. The experimental results used to determine all the TEC performance parameters can be measured virtually. The thermoelectric module TEC1-12706 made by Tianjin Institute of Power Sources, China, is chosen in this section as the simulation example because the detailed temperature dependences of the *n*- and *p*-type bismuth telluride materials are available from the manufacturer. The thermal and electrical contact resistances of TEC1-12706 are also experimentally determined in the previous study [30].

Unless a uniform distribution is imposed, the temperature profile of TEC ceramic surfaces is usually non-uniform primarily due to the space between TE elements within the module, as is shown in Fig. 5(c). Therefore, in dealing with the ΔT information associated with the physical model, the arithmetic average of the temperatures of all cell faces at the TEC surface, calculated automatically in the UDF, is actually plotted in the following figures.

The squares in Fig. 6(a) present the physical simulation of the change of ΔT with I when $\dot{Q} = 0$ W. It can be seen that $\Delta T_{max} = 57.63$ K occurs at the current $I_{max} = 5.7$ A. $\dot{Q}_{max} = 51.25$ W can be obtained by another simulation in which I_{max} is applied and the both sides of the TEC prescribed to be the same temperature. In terms of (24)-(26), the effective α, ρ, κ can be obtained for the compact TEC model, as is shown in Fig. 5(b).

Fig. 6(a) and (b) show clearly that the physical model and the compact model depict the ΔT change as a function of I with almost the same characteristics. The small difference between the two simulations is slightly enlarged when the thermal load is increased, similar to the results presented in Section 2. In Fig. 7(a) and (b), the changes of V with I by the physical model and the compact model are compared under different thermal loads. For most current values, it can be seen that the two models match very well. When $\dot{Q}$ is increased and when I passes its maximum value, once again, the deviation becomes more obvious as the results in Section 2. It is noteworthy that, when $I > I_{max}$, the $V - I$ curves from the physical

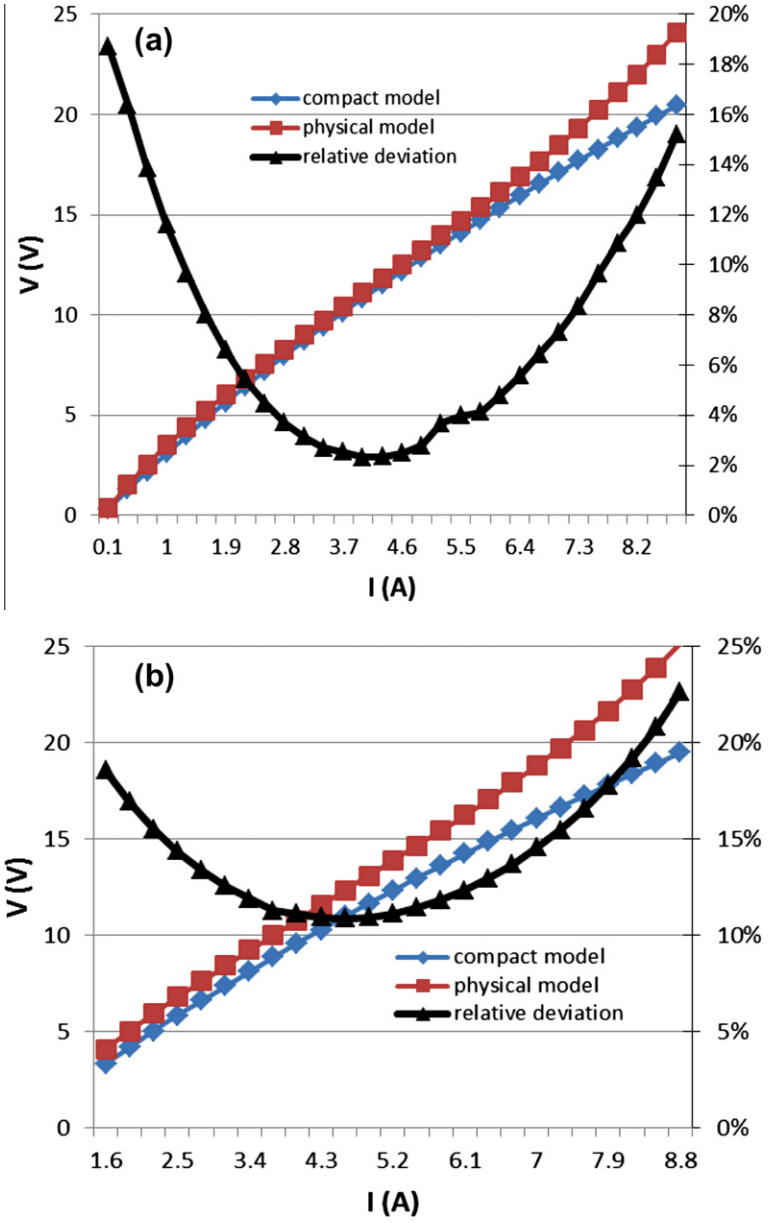

Fig. 7. TEC power supply voltage comparison between compact simulation and full simulation for various currents (a) $\dot{Q} = 0$ W, $T_h = 300$ K; (b) $\dot{Q} = 20$ W, $T_h = 300$ K.

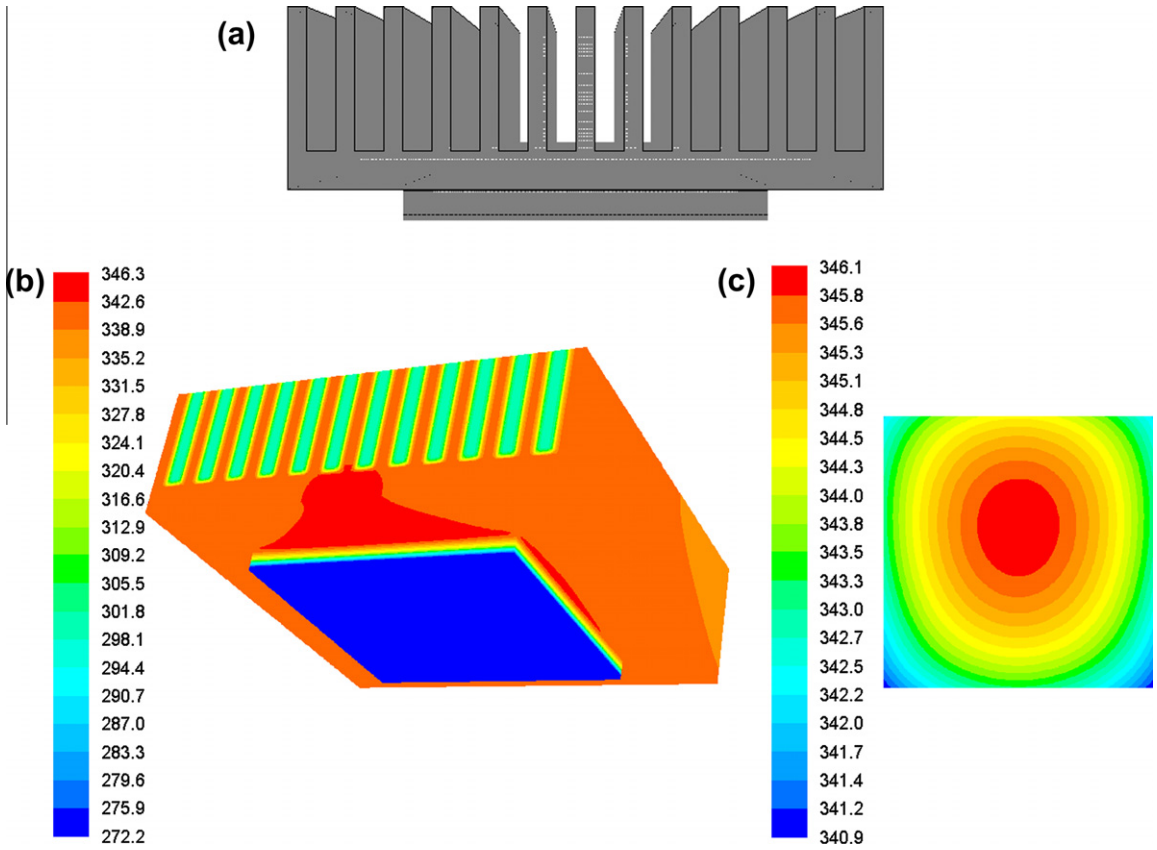

Fig. 8. TEC based heat sink of a cooling system using the compact CFD model, (a) schematic structure and dimension, (b) 3D temperature distribution, (c) 2D temperature distribution of the TEC hot side surface, ($\dot{Q} = 0$ W, $I = 5.7$ A, velocity: 30 m/s).

model shows a nonlinear change, which cannot be accurately captured by the compact model. As explained above, the physical model faithfully reflects the temperature dependent material properties and the full coupled multi-physics effects. The relative deviations between the two models are also given in Fig. 7, and it can be seen that the relative deviations are actually within the normal range when the absolute deviation is enlarged at extremely high currents.

The temperature variation within the entire surface by the compact model is very small (265.91 ± 0.01 K), as shown in Fig. 5(b). In Fig. 5(c) where the local range of the 2D TEC cold side is applied to the temperature scale, the physical model clearly displays its excellent ability to accurately capture the horizontal temperature gradient caused by the heat spread [31], which is very useful in analyzing spot cooling applications. Therefore, in situations when the computation accuracy of unusual situations is highly demanded the physical model is likely to be more accurate than the compact model.

On the other hand, the compact model can display its strength when computational cost and efficiency are taken into account. Regarding modeling size, the FLUENT computational domain of the physical TEC model contains 658,495 volumes and 881,900 nodes, whilst the compact TEC model has 121,600 volumes and 143,702 nodes. In order to speed up the convergence of the potential field, double-precision solver (3DDP) is used for the physical model instead of a single precision solver, and on a Lenovo W520 laptop workstation, the model takes approximately 10 h in average to finish the computation. However, the compact TEC model takes only a few minutes to converge on the same computer when 3DDP is selected due to the simplification on both gridding and computing. Thus, in many scenarios of cooling system optimization where the computation efficiency is an important factor, a sensible trade-off between the accuracy of the physical model and the speed of the compact model should lead to selection of the compact model given their small simulation differences under normal applications as shown in Fig. 6 and 7.

4. Model exploration at the system-level

While the processes and phenomena within a TEC are complex, its compact model has a straightforward and feasible path to thermal management applications when all the important effective parameters are appropriately extracted. To provide a clear description how the compact model is applied to the design of practical cooling systems, an assembly comprising a TEC and an air cooled heat-sink is modeled in FLUENT. As is shown in Fig. 8(a), the TEC is assumed mounted on a component, and the bottom surface of the TEC represents the heat source on which either a heat flux or a temperature can be specified. It is assumed that air flows through the duct and fins of the heat sink so that it cools the TEC by forced air convection.

In the CFD model, the finned geometry of the heat sink, as an empirical design, indicates the presence of laminar airflow. A constant inlet temperature of 300 K and a number of air velocities were considered as fluid dynamic boundary conditions. Thermal boundary conditions on other walls that are not attached to the heat source or exposed to the airflow are assumed adiabatic. In the simulation of such a cooling system, the inputs are the inlet air velocity and temperature, the source temperature/heat generation rate, the electrical current to the TEC, and the outputs are the 3D temperature and flow fields of the whole computation domain, as is shown in Fig. 8(b).

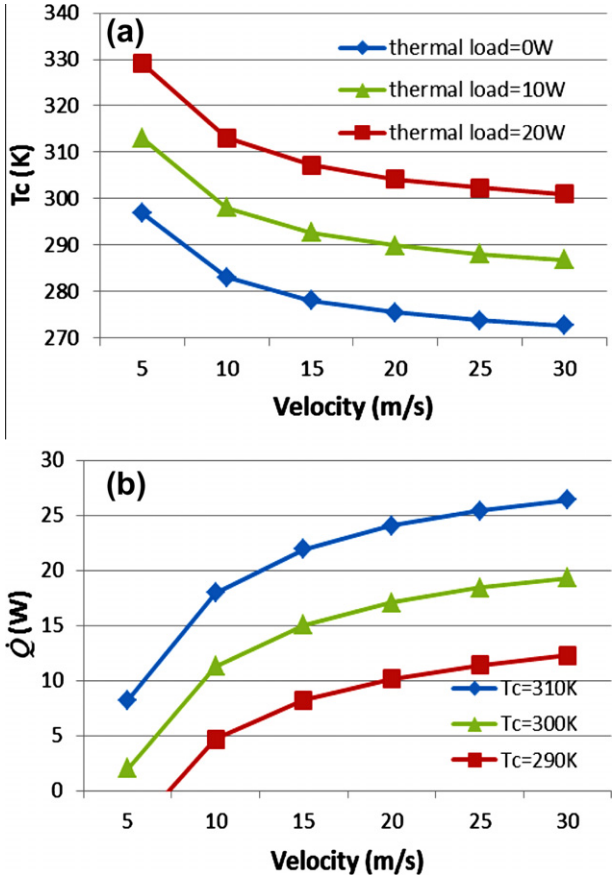

Fig. 9. TEC cold side temperatures (a) and thermal loading ability (b) for various airflow velocities (I = 5.7 A).

In the 3D temperature contour, it can be seen that there is an obvious temperature gradient from the flow (outlet) to the heat sink base due to the small thermal resistance of the heat sink. The TEC enables an "active" heat sink by reducing the cooling temperature below the ambient (300 K). The effect of the air flow on the 2D temperature distribution of the base surface in the heat sink is shown in Fig. 8(c), which displays a non-uniform profile.

Fig. 9(a) shows how the temperature of the TEC cold side can be reduced by increasing the airflow velocity to enhance the convection. It can be seen that the optimal velocity is around 10 m/s for various thermal loads, and when the velocity is higher than 15 m/s, further enhancement of the convection cannot significantly improve the cooling performance. Similarly, the heat pumping ability from the cooling objective to the flow fluid of the heat sink is optimized within the range 5–15 m/s, after which the thermal load cannot be significantly increased, as is shown in Fig. 9(b).

5. Conclusions

This paper presents a compact 3D TEC model by which the different materials and components within the TEC module are abstracted as a single block. A significant amount of grid is reduced in modeling a TEC, and also the grid size mismatch between the TEC and thermal system is mitigated. It is also shown how the effective parameters of the compact model can be extracted from manufacturer's data or calculated from materials parameters. The compact model and parameter extraction are validated by comparing the simulation results and the manufacturer's performance data at various electrical and thermal conditions with excellent agreement.

A full TEC model is also implemented in FLUENT, where the exact device geometry, coupled thermoelectric effects, and the thermal gradient and electric potential are fully represented in 3 dimensions. The physical model can be used to carry out virtual experiments to obtain TEC performance data to extract the effective parameters for the compact model. Simulation comparisons validate that the compact modeling and parameter extraction yield results almost as accurate as the physical model, but with computational speed roughly 100 times faster.

The compact model uses the CFD approach, so that the integration of TEC into many thermal management applications can be readily implemented. A demonstrative example of successful utilization of the compact model is presented by modeling an air-cooled heat sink. Rapid optimization of the cooling system, e.g., fan arrangement, airflow speed and angle, fin and spreader geometry, as well as the TEC operating current, can be done in a systematic way. A detailed comparison of various spacing, length, and width of the fins to enhance the heat transfer for TEC applications, taking advantage of the proposed co-simulation technique, can be found in [32].

Acknowledgements

We thank AFOSR MURI FA9550-10-1-0533, and NASA-JPL for support. Min Chen is also supported by DFF FTP 09-069739 and AAU Kompetencefonden in connection with his research stay at Caltech.

References

[1] G.J. Snyder, J.-P. Fleurial, R-G. Yang, T. Caillat, G. Chen, Supercooling of Peltier cooler using a current pulse, J. Appl. Phys. 92 (2002) 1564.
[2] R.E. Simons, M.J. Ellsworth, C. Chu, An assessment of module cooling enhancement with thermoelectric coolers, ASME J. Heat Transfer 127 (2005) 76–84.
[3] K. Yazawa, G.L. Solbrekken, A. Bar-Cohen, Thermoelectric-powered convective cooling of microprocessors, IEEE Trans. Adv. Packag. 28 (2005) 231–239.
[4] R.A. Khire, A. Messac, S.V. Dessel, Design of thermoelectric heat pump unit for active building envelope systems, Int. J. Heat Mass Transfer 48 (2005) 4028–4040.
[5] R.A. Taylor, G.L. Solbrekken, Comprehensive system-level optimization of thermoelectric devices for electronic cooling applications, IEEE Trans. Compon. Packag. Technol. 31 (2008) 23–31.
[6] A. Sinha, Y. Joshi, Application of thermoelectric-adsorption cooler for harsh environment electronics under varying heat load, ASME J. Therm. Sci. Eng. Appl. 2 (2009) 021004.
[7] P. Naphon, S. Wiriyasart, Liquid cooling in the mini-rectangular fin heat sink with and without thermoelectric for CPU, Int. Commun. Heat Mass Transfer 36 (2009) 166–171.
[8] H. Huang, Y. Weng, Y. Chang, S. Chen, M. Ke, Thermoelectric water-cooling device applied to electronic equipment, Int. Commun. Heat Mass Transfer 37 (2010) 140–146.
[9] E. Elena, D.C. Looman, Finite elements for thermoelectric device analysis in ANSYS, in: Proceedings of 24th International Conference on Thermoelectrics, Clemson, USA, 2005, pp. 200–203.
[10] K.H. Lee, O.J. Kim, Analysis on the cooling performance of the thermoelectric micro-cooler, Int. J. Heat Mass Transfer 50 (2007) 1982–1992.
[11] C. Cheng, S. Huang, T. Cheng, A three-dimensional theoretical model for predicting transient thermal behavior of thermoelectric coolers, Int. J. Heat Mass Transfer 53 (2010) 2001–2011.
[12] J. Pérez-Aparicio, R. Palma, R. Taylor, Finite element analysis and material sensitivity of Peltier thermoelectric cells coolers, Int. J. Heat Mass Transfer 55 (2012) 1363–1374.
[13] Junior, G. Chen, J. Koehler, Modeling of a new recuperative thermoelectric cycle for a tumble dryer, Int. J. Heat Mass Transfer 55 (2012) 1536–1543.
[14] M.P. Codecasa, E. Colombo, F. Inzoli, G. Pastorino, C. Rizzo, Optimization of a new thermoelectric cooling assembly using CFD analysis and local modeling of thermoelectric effects, in: Proceedings of 22nd International Conference on Thermoelectrics, Herault, France, 2003, pp. 614–618.
[15] M. Chen, L.A. Rosendahl, T. Condra, A three-dimensional numerical model of thermoelectric generators in fluid power systems, Int. J. Heat Mass Transfer 54 (2011) 345–355.
[16] E. Prather, B. Puranik, Three-dimensional simulation of thermoelectric devices with compact numerical models, in: Proceedings of International Electronic Packaging Technical Conference and Exhibition, Hawaii, USA, 2003, pp. 335–342.

[17] K.V. Karimanal, M.J. Ellsworth, G. Refai-Ahmed, A numerical technique for modeling thermoelectric cooler with temperature controller for steady state CFD applications, in: Proceedings of ASME International Mechanical Engineering Congress, Washington D.C., USA, 2003, pp. 245–251.
[18] M. Gonzalez, E. Arguelles, J. Rodreguez, M. Garcia, Thermal performance of a controlled cooling system for low-level optical signals, Appl. Therm. Eng. 24 (2004) 2041–2054.
[19] I. Sauciuc, H. Erturk, G. Chrysler, V. Bala, R. Mahajan, Thermal devices integrated with thermoelectric modules with applications to CPU cooling, in: Proceedings of ASME 2005 Pacific Rim Technical Conference and Exhibition on Integration and Packaging of MEMS, NEMS, and Electronic Systems, San Francisco, USA, 2005, pp. 2149–2155.
[20] N. Lakhkar, M. Hossain, D. Agonafer, CFD modeling of a thermoelectric device for electronics cooling applications, in: Proceedings of 11th Intersociety Conference on Thermal and Thermomechanical Phenomena in Electronic Systems, Orlando, USA, 2008, pp. 889–895.
[21] M. Pearse, Modelling methodology for thermo-electric coolers in CFD, in: Proceedings of 2nd Electronics System-Integration Technology Conference, Greenwich, UK, 2008, pp. 1171–1174.
[22] Q. Nie, Y. Joshi, Multiscale thermal modeling methodology for thermoelectrically cooled electronic cabinets, Numer. Heat Transfer A 53 (2008) 225–248.
[23] M.P. Gupta, M. Sayer, S. Mukhopadhyay, S. Kumar, Ultrathin thermoelectric devices for on-chip Peltier cooling, IEEE Trans. Compon. Packag. Manuf. Technol. 1 (2011) 1395–1405.
[24] S. Lineykin, S. Ben-Yaakov, Modeling and analysis of thermoelectric modules, IEEE Trans. Ind. Appl. 43 (2007) 505–512.
[25] S. Lineykin, S. Ben-Yaakov, User-friendly and intuitive graphical approach to the design of thermoelectric cooling systems, Int. J. Refrig. 30 (2007) 798–804.
[26] F.L. Tan, S.C. Fok, Methodology on sizing and selecting thermoelectric cooler from different TEC manufacturers in cooling system design, Energy Convers. Manage. 49 (2008) 1715–1723.
[27] H.N. Phan, D. Agonafer, Thermoelectric cooling analysis using modified-graphical-method for multidimensional-heat-transfer-system, ASME J. Electron. Packag. 133 (2011) 031003.
[28] A.F. Ioffe, Semiconductor Thermoelements and Thermoelectric Cooling, Infosearch Limited, London, 1957.
[29] Marlow industries inc., Thermoelectric Cooler Datasheet DT12-4.
[30] M. Chen, L.A. Rosendahl, T.J. Condra, J.K. Pedersen, Numerical modeling of thermoelectric generators with varying material properties in a circuit simulator, IEEE Trans. Energy Convers. 24 (2009) 112–124.
[31] K. Yazawa, A. Shakouri, Cost-efficiency trade-off and the design of thermoelectric power generators, Environ. Sci. Technol. 45 (2011) 7548–7553.
[32] X. Gao, M. Chen, G.J. Snyder, S.J.Andreasen, S.K.Kær, Thermal management optimization of a thermoelectric-integrated methanol evaporator using a compact CFD modeling approach, Journal of Electronic Materials (2013). http://dx.doi.org/10.1007/s11664-013-2514-2.